Composite Structures 292 (2022) 115678

Contents lists available at ScienceDirect

Composite Structures

journal homepage: www.elsevier.com/locate/compstruct

Experimental analysis of fiber-reinforced laminated composite plates with embedded SMA wire actuators

Andrew J. Theodore, Peter L. Bishay *

Department of Mechanical Engineering, California State University, Northridge, United States

ARTICLE INFO

Keywords:
Shape memory alloy
Laminated composites
Smart materials
Active structures

ABSTRACT

Shape memory alloy (SMA) wires are effective smart actuators since they provide relatively large actuation force and strain in a very limited space. Embedding SMA wires in flexible laminated composite plates or shells allows for creating active structures for morphing applications. However, the design of such structures is challenging due to the nonlinear thermomechanical coupling of SMA materials, the adhesion of the SMA actuators to the resin, the effect of temperature on the adhesion strength, the heat transfer between the SMA wires and the surrounding laminate, and the convection boundary conditions. This paper presents an experimental analysis of smart fiber-reinforced composite laminated plates with embedded SMA wires, focusing on the relationship between the applied electric current, measured temperature of the SMA wires, and the resulting tip deflection. A temperature-based control method was developed to achieve the required wire temperature and tip deflection as quickly as possible. Results showed that the fiber-orientation angle of the composite plies and the convection boundary conditions have significant effects on the structure's actuation. With cyclic actuation, damage starts around the heated SMA wires and can grow to cause delamination at areas between neighboring SMA wires and yielding of the matrix material, resulting in permanent deformation.

1. Introduction

Shape memory alloy (SMA) actuators have been introduced to a wide range of engineering applications, such as morphing wings [1–3], soft robotic grippers [4,5], and prosthetic arms [6,7]. Laminated composites with embedded SMA wires have been developed and tested in the last two decades, introducing new characteristics to the host structures. Due to their unique mechanical properties and actuation capability, SMAs can act as additional means of reinforcement to structures subjected to specific types of loads, or can actuate some structures in morphing and shape-changing applications. Generally, passive applications involve SMA wires placed such that the wires' center axes are in-plane with the laminate's neutral axis [8]. For example, Ellis [9] showed that incorporating SMA wires into graphite epoxy laminates could increase low velocity impact energy absorption by 99% while only increasing the total laminate mass by 12%. Guida *et al.* [10] performed experimental and numerical testing on a Kevlar fabric reinforced thermoplastic composite laminate with embedded SMA wires in a leading edge of a wing. The composite with SMA wires showed higher toughness and absorbed more impact energy due to its superelastic and hysteretic properties. SMA wires have also been embedded in composites for passive vibration control applications. Pappada *et al.* [11] found that embedding SMA wires into composite laminates, especially those that have been prestrained to take full advantage of hysteresis associated with hybridization, increases the internal damping ratio of the composite structure. Analytical models of concrete beams with embedded SMA rods, and functionally graded or laminated composite beams with embedded SMA layers were developed by Zaki and co-workers [12–14]. The influence of the applied temperature, as well as the smart beam's geometric and material properties on the bending response and superelasticity, were investigated.

SMA wires have also been embedded in resins to realize self-healing polymeric structures. Kirkby *et al.* [15] injected a healing agent into cracks in polymeric test samples before contracting the embedded SMA wires via resistive heating for 30 min. After the healing process, the polymer test samples recovered 98% of their original strength. In a later work, Kirkby *et al.* [16] incorporated microencapsulated liquid healing agents into the cured polymer. Upon cracking, the liquid healing agent contacted a solid catalyst also embedded into the polymer. The SMA wire was then activated to close the crack and to provide a clamping

* Corresponding author.
E-mail address: peter.bishay@csun.edu (P.L. Bishay).

https://doi.org/10.1016/j.compstruct.2022.115678
Received 27 August 2021; Received in revised form 12 November 2021; Accepted 24 April 2022
Available online 28 April 2022

force and heat to reduce the cure time of the healing agent.

SMAs can be embedded in smart soft composites used in a variety of applications. For example, shape morphing of flexible composite structures can be achieved by placing SMA wires offset from the laminate's neutral axis, such that stresses developed in the wires exert internal bending moments [8]. Han *et al.* [17] designed morphing winglets constructed of woven glass fabric, a polydimethylsiloxane (PDMS) elastomer matrix, and embedded SMA wires. The active ply with SMA wires was reinforced with interwoven glass fibers. They investigated the wings' aerodynamic performance with wind tunnel testing. Testing showed that the structure was capable of large displacements sufficient to positively affect the wing's aerodynamic performance, while maintaining adequate stiffness and strength to resist the aerodynamic loads without damage from repeated actuation. In a follow up work, Han *et al.* [18] manufactured and tested morphing composite plates with SMA wires embedded in multiple directions. Similar to prior test laminates, the active plies featured SMA wires woven with E-glass and nylon fibers. The effects of varying the orientation between active and fiber-reinforced plies in addition to varying the number of plies were investigated. The laminates were capable of multidirectional control via separate SMA wire circuits. The weaving method was found to have an influence on the deformation of each plate. Leal *et al.* [23] designed and tested a camber morphing wing design that incorporated SMA wires as actuators in a PDMS elastomer insert which was embedded in a machined polyethylene and polystyrene foam core. This design was unique in that the SMA wires were weaved around steel dowels which were molded into the foam structure. This way, loads were transferred to the wing structure through the dowels rather than relying on transferring shear to the surrounding matrix. Kim *et al.* [20] developed a prosthetic hand based on an artificial finger design as a smart soft composite (SSC) actuated using embedded SMA wires. A sensitivity analysis was conducted on this design to investigate the effect of different design parameters on finger deformation [21]. SMA-actuated morphing structures have also been used in applications involving soft robotics. Jin *et al.* [24] constructed and tested a modular soft robot that used SMA wire actuators embedded in a PDMS structure. The SMA wires produced a bending moment in the structure by applying load to an end plate, rather than by directly transferring shear to the matrix material. Wang *et al.* [25] proposed a novel design which incorporated embedding support ribs composed of a fusible alloy structure into a morphing composite structure which are melted at relatively low temperatures by Joule heating. This design eliminates the need to provide constant current to the wires to control the position of the structure, significantly reducing the energy requirement of a structure that does not need to constantly change shape. Daghia [22] presented a detailed experimental study on the manufacturing and actuation of an S-glass/polyester resin composite with embedded prestrained SMA wire actuators. Choyal *et al.* [19] recently presented an experimental investigation of the actuation behaviour of SMA-based adaptive composite plates. Various SMA wire configurations and diameters were considered and samples were tested under multiple heating and cooling cycles. The study showed the effect of the convection boundary conditions on the plate's tip deflection.

To develop a realistic technology that incorporates composite materials with embedded SMA wires, failure modes need to be well understood. Lau *et al.* [26] made microscale observations with scanning electron microscopy (SEM) to produce images of cracks formed at the interface between an SMA wire and an epoxy matrix. The results showed that disbonding began to occur as the prestrain of the SMA wire increases, forming small cracks near the wire/matrix interface. Yuan *et al.* [27] investigated means of improving the bond interface between the matrix material and the SMA wires by mechanically indenting the SMA wires with specialized tooling. It was found that the interface strength was improved by up to 4.5 times when compared to SMA wires that were hand sanded only. In another paper, Yuan *et al.* [28] investigated the deflection of a cantileverd composite beam with indented SMA wires embedded in a glass fiber reinforced laminate.

This paper presents an experimental investigation of the cyclic actuation and damage in composite laminates with embedded SMA wires. The rest of the paper is organized as follows: material selection is covered first in Section 2, and manufacturing steps are then detailed in Section 3, followed by a mathematical model to estimate the embedded SMA wire temperature in Section 4. Section 5 presents the test setup and measurement tools, and then the experimental results are presented in Section 6. Finally, conclusions are summerized in Section 7.

2. Material selection

As reported by Lester *et al.* [29], many polymers have been proposed to be used as a matrix material in composite systems with embedded SMA actuators. There are a number of material properties required in a morphing composite structure capable of large deflections. First, the matrix material needs to be capable of undergoing at least as much strain as the undeformed prestrain level in the embedded SMA wires, typically around 4–5%. Materials that are too brittle and stiff result in interfacial debonding at the SMA wire/polymer interface, such as that observed by Merlin *et al.* [30] in polyester (PE) and vinyl ester (VE) matrix composites. In other words, the matrix materials used in morphing composites need to have a high yield strain, defined as the ratio between the yield strength and Young's modulus of the material, and therefore stiff materials could be suitable if they have a corresponding high yield strength. A high concentration of embedded SMA wire actuators may be necessary with a stiffer matrix to overcome the higher strain energy requirement to achieve morphing. Matrix materials used in composite structures with embedded SMA wires also need to be electrically insulating to ensure current flows only through the SMA wires and supplies uniform heating.

Rhino 1382 low modulus flexible epoxy resin [31] was chosen in this work because it meets the criteria of having a high yield strength and low stiffness. It cures using Rhino 3182 "impact-resistant" hardener. This flexible epoxy is advertised as being capable of up to 50% elongation, which makes it suitable for flexible composites. The curing temperature range is 12–30 °C. Resistance measurements across the embedded SMA wire confirmed that this epoxy has near perfect electrical insulation over the relatively low voltage range used in testing. The results presented later in this paper also shows that this epoxy provided excellent adhesion to the SMA wire using only simple surface preparation techniques.

The fibers or the reinforcing agent also needs to be electrically insulating and have a high yield strain. Carbon fibers, which are brittle and electrically conductive, are difficult to implement in morphing composites structures with embedded SMA wire actuators. It has been noted that Kevlar's negative thermal expansion coefficient relieves stress mismatch at the interface between the fibers and SMA wires and shifts the debonding temperature to a higher value [32]. Additionally, Kevlar fibers are electrically insulating and capable of ultimate strains generally higher than that of carbon fibers, but lower than glass fibers [33]. They are lighter than glass fibers, yet are much stiffer and stronger. They have high ultimate tensile strengths, comparable to carbon fibers, but are less brittle due to their unique molecular structure [34]. Kevlar fibers have been cited to have a high susceptibility to moisture-related degradation in performance, a major obstacle for its implementation in applications such as aircraft or automobile external surfaces that are exposed to water directly. HexForce™ 7715 is a unidirectional fiberglass cloth constructed of E-glass fibers stitched together with smaller reinforcing fibers that are only intended to hold the main fibers aligned. These fibers were selected for use in the test samples manufactured in this work. Unidirectional cloth was chosen so that the angle between the fibers and embedded SMA wires could specifically be controlled. The orthotropic properties of unidirectional cloth allow for the opportunity to minimize the bending stiffness. These commercially available fibers are electrically insulating and provided high yield strain.

FLEXINOL is a trade name for Nickel Titanium (NiTi) alloy that

exhibits shape memory and pseudoelastic behavior (Dynalloy, Inc.). Wire with a 0.38 mm diameter and austenite finish occurring around 70 °C in the stress-free condition was selected to minimize the operating temperature in an effort to prevent damage to the flexible epoxy matrix. Epoxies in general have a large operating range of around 50 – 120 °C, mainly based on the specific chemical composition and preparation of the epoxy [35]. For this reason, wire temperatures were maintained below approximately 80 °C to prevent damage to the epoxy matrix. Under stress, the wire transformation temperatures increase. Applying a tensile load of 69 MPa at room temperature elongates the material axially by about 4–5%. This level of strain is recoverable for hundreds of thousands of cycles if recovery stress remains below 100 MPa. The yield strength of the material in the austenitic phase is given by the supplier to be at least 345 MPa. Operating at stresses 67% of this yield stress level or above results in rapid degradation of the material's shape memory ability and causes permanent deformation. Similarly, operating at initial prestrain levels above 5% results in quicker degradation of the material's shape memory ability and permanent deformation after relatively few cycles. The wire is supplied with a minimum prestrain of 4% and is in a stable trained condition.

Many authors have documented difficulties associated with adhering or bonding SMA wires to various polymer matrices. Merlin *et al.* [30] used chemical etching and a silane coupling agent. Smith *et al.* [36] coated the SMA wires with black oxide and silane surface treatment. Jonnalagadda [37] used test specimens with a sandblasted surface. Rey *et al.* [38] recommended the use of an adhesion primer Bluesil PM820 and plasma surface finish treatment. The SMA wires embedded in the test laminates in this work were thoroughly sanded with 220 grit sandpaper prior to lamination. This process removed a naturally occurring oxide layer and roughened the wire surface. The wire was then degreased by submerging in pure acetone for 15 min. After cleaning, the wire was then only handled with gloves and stored in a dry plastic bag.

3. Manufacturing

To accurately position the SMA wire within the laminate, the fixture shown in Fig. 1 was used. The SMA wire was looped and clamped to the plate using socket head cap screws. The wire was then laced over equally spaced dowel pins pressed into the aluminum plate. Tension was applied to the wire during this process to eliminate slack, which resulted in better wire alignment. Various wire spacings can be achieved by varying the wire lacing pattern used. The matrix material was mixed per its respective manufactures' recommended proportions. A wet layup technique was used to manufacture the sample laminates. Fiberglass plies were placed above or below the wires, in the flat area between the pins, according to the stacking sequence of each laminate. All laminates were manufactured as square plates having a nominal length and width of 100 mm. Fig. 2 shows the sealed layup with vacuum applied during curing. After curing, the laminate was released and trimmed to the nominal dimensions. The evenly spaced wire segments were approximately centered to the plate midline, with the first and tenth wires 5 mm from each edge. Kapton tape and wire leads were installed to prepare the plate for testing, as shown in Fig. 3. The tape was used to prevent accidental electric shorting between adjacent exposed wire loops or with the test fixture. The wire leads were added to allow for easy attachment of alligator leads to the wires.

Fig. 1. SMA wire placement fixture used for manufacturing test laminates.

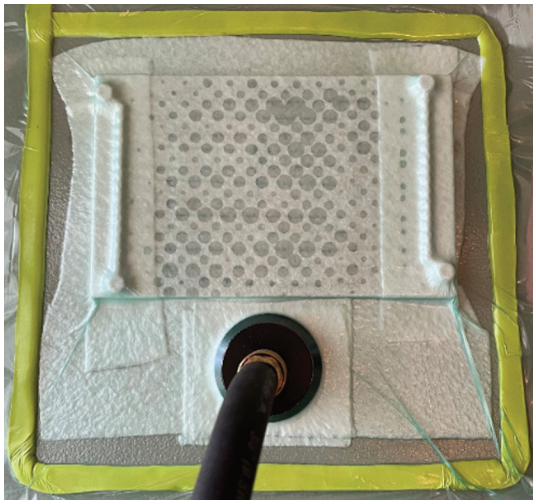

Fig. 2. Laminate curing with vacuum applied by a pump.

A total of three test samples were manufactured and tested. The number of embedded SMA wires and the physical dimensions were held constant to isolate the effects of fiber ply orientation. Laminates 1, 2 and 3 had [90°/W/-45°/45°], [90°/W/-60°/60°] and [90°/W/90°/90°] stacking sequences respectively, where "W" in the laminate code indicates SMA wires at 0°. Laminate 3 had all fibers perpendicular to the SMA wire and had the minimum bending stiffness in the actuation direction. The fibers in laminate 2 were aligned such that the bending stiffness was greater than laminate 3, but less than laminate 1.

4. Joule heating of embedded SMA wires

Most applications involving SMA wire actuators use Joule heating to heat the wires past their transformation temperatures to induce strain recovery in the material. Joule heating of a metallic wire can be expressed using the differential equation,

$$T(t) = \frac{R}{h_c A_c} i^2 \left(1 - e^{-t/t_h}\right) + T_\infty \tag{1}$$

where R is the total wire resistance, h_c is the convection coefficient, A_c is the wire circumferential area, i is the applied current, T_∞ is the ambient temperature, and t_h is the time constant expressed as.

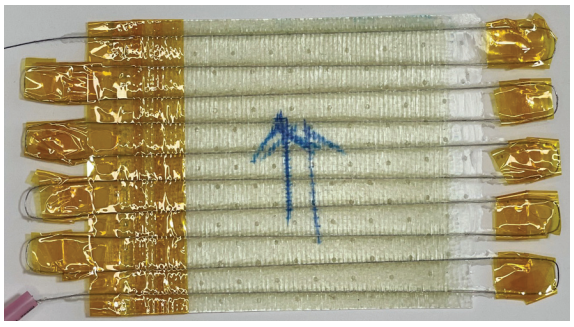

Fig. 3. Test laminate shown after trimming and installation of Kapton tape and wire leads.

$$t_h = \frac{\rho A c_p}{h_c A_c} \tag{2}$$

where ρ is the density of the wire, A is the cross-sectional area, and c_p is the specific heat of the wire.

The steady state temperature can then be obtained when the exponential term vanishes as:

$$T_{SS} = \frac{R}{h_c A_c} i^2 + T_\infty \tag{3}$$

A value for the convection coefficient can be experimentally determined by measuring all terms on the right hand side of this equation, as,

$$h_c = \frac{i^2 R}{A_c (T_{SS} - T_\infty)} \tag{4}$$

The value achieved by this method is assumed to capture the convection heat losses over the laminate total area, provided by a conductive path through the matrix to the embedded wires.

A layer of insulation was required between the bare SMA wire to prevent current in the wire heating circuit from flowing into the data acquisition circuit. Consequently, a temperature drop occured across the insulation layer, which can be modeled using [39]:

$$T_i = \frac{\dot{e}_{gen} r_1^2}{2 k_{ins}} \ln\left(\frac{r_2}{r_1}\right) + T_s \tag{5}$$

where T_i is the interface temperature between the wire and insulation, $\dot{e}_{gen}$ is the power generated per unit volume, k_{ins} is the thermal conductivity of the insulation material between the thermocouple and the wire, and T_s is the temperature measured by the thermocouple. The radius of the wire r_1 and the radius of the insulation layer r_2 are shown in the schematic of Fig. 4.

With the interface temperature between the wire and insulation known, the temperature of the center of the wire can be calculated as:

$$T_{wire,\,center} = T_i + \frac{\dot{e}_{gen} r_1^2}{4 k_{wire}} \tag{6}$$

where k_{wire} is the thermal conductivity of the wire. While this approach is relatively simple, measurement of wire temperature with a thermocouple is further complicated when the thermocouple tip is approximately the same size as the SMA wire's cross-sectional area, as Daghia [22] and others reported.

In the case of the geometry shown in Fig. 4, the distance between the thermocouple tip and the SMA wire is only equal to r_2 at a single point and greater than r_2 everywhere else. Also, the gap between the thermocouple and wire is predominately insulated by air, rather than the Kapton tape. Daghia [22] noted that micrometric thermocouples (i.e., thermocouples that are very small relative to the SMA wire) embedded directly into the composite provide better measurements for temperature control. This is because the distance between the SMA wire and the thermocouple tip is approximately the same at all locations, in addition to the reduced transient effects associated with heating additional mass. Various thermocouple arrangements were tested to improve the temperature measurements obtained. The configuration shown in Fig. 5 resulted in the most consistent temperature measurements with the least temperature drop.

Equation (6) was applied to estimate the true wire temperature. The quality of that estimate is highly dependent on the accuracy of the value used for k_{ins}. If the primary objective is to ensure phase transformation, it may be best to assume a more conservative value that results in a smaller estimated temperature drop.

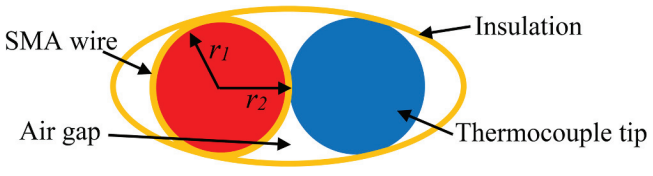

Fig. 4. Approximate geometry of case with thermocouple and wire wrapped in Kapton tape.

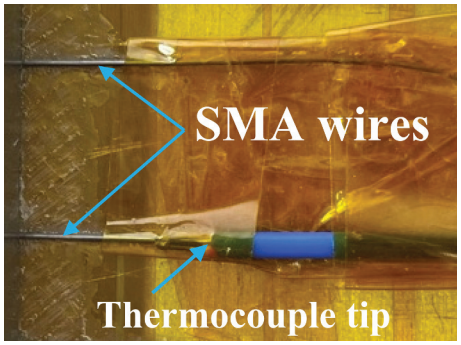

Fig. 5. Thermocouple tip on wire external to epoxy wrapped in Kapton tape.

5. Test setup and measurements

The performance of a morphing composite structure depends on robust electronics as much as it depends on an efficient mechanical design. The same tool used for the laminate layup process was also used as a test fixture in all deflection tests of the manufactured samples. Each test plate was clamped at one edge, as shown in Fig. 6, to achieve a cantilever configuration. The clamped edge was wrapped in Kapton tape to prevent the clamp from damaging the laminate and shorting the wires. Alligator clips were attached to the test leads crimped onto the SMA wire ends, with one lead connected to a DC power supply and the other connected to the current control circuit, shown in the schematic in Fig. 7.

This circuit was used to collect current, temperature, and voltage data in all tests presented here. In addition to data acquisition, the circuit also functioned as a programmable closed-loop control system. A variable DC voltage source provided voltage ranging from 0 to 30 V. The SMA wire embedded in the composite was modeled as a resistor, represented by R_{SMA} in the schematic. An Arduino Uno microcontroller read analog voltage data output by the thermocouple amplifier and current sensing chips. The metal–oxide semiconductor field-effect transistor (MOSFET) acted as a current regulator and was controlled by varying the voltage at its gate via pulse-width modulation (PWM). The PWM method enabled current control via a digital voltage signal output by the Arduino microcontroller. A 10 kΩ pulldown resistor was attached

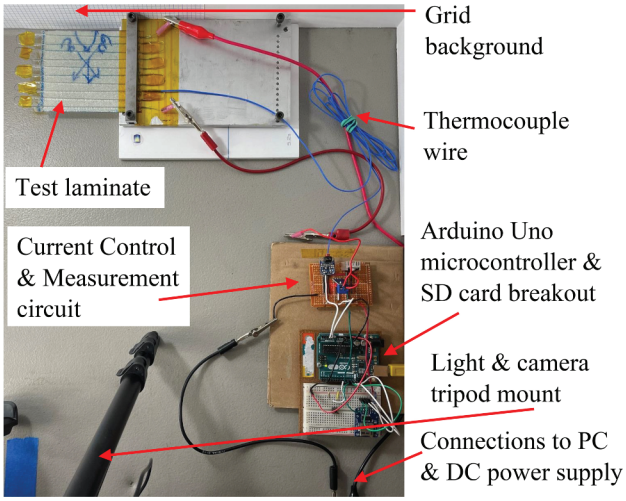

Fig. 6. Photo lab and test instrumentation used for data collection.

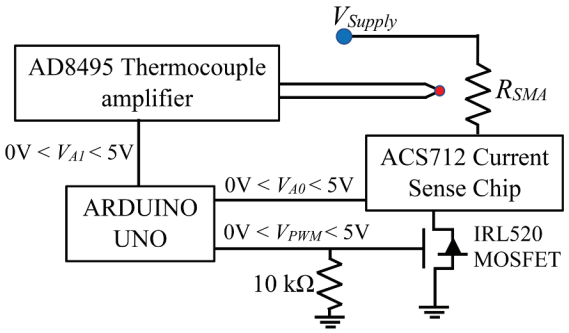

Fig. 7. SMA wire current control circuit schematic.

between the gate pin and ground to ensure the voltage signal is zero when the PWM signal is zero or OFF. The use of a programmable microcontroller allowed for various modes of operation during testing. The control method was implemented via programmable script written in Arduino language, which was uploaded to the microcontroller prior to testing.

The implemented control method used temperature data and an input room temperature value to calculate temperature differential ΔT between the measured SMA wire temperature and ambient air. The difference between this measured ΔT value and a user input ΔT value was used to calculate the amount of current required to achieve the setpoint, T_{SS}. A negative-feedback, closed-loop control method was used such that maximum current was applied at room temperature, which decreased to zero as the measured temperature approached the setpoint. This control scheme could be tuned for various austenite finish temperatures to assure transformation is completed in the wire.

Deflection measurements were recorded by visual inspection methods in all tests. The complete test setup is shown in Fig. 6. An iPhone camera was placed on a tripod and was used to record all raw image and video files. The phone's internal leveling app was used to ensure the camera lens was level relative to gravity, measured by the phone's internal accelerometer. The camera was then squared against a 2D grid placed behind the test sample using a large L-square. Measurement error in tip deflection due to angular misalignment between the camera and the laminate edge was negligible considering small-angle approximation.

6. Results

6.1. Constant voltage test

The goals of this test were to know the limits of the structure by increasing the constant voltage applied on the embedded SMA wire and to observe the damage that may occur. Only laminate 1 was tested here. The three tests performed on this sample are summarized in Table 1. The ON times shown in the first two tests were variable in order to reach steady-state deflection at the shown voltages. After reaching steady-state deflection values, the current was switched off.

Initially, 12 V was applied for 35 s until the measured temperature reached about 40 °C. The voltage was then increased to 16 V in test 1, inducing 1.0 A of current and heating the wire to a maximum measured temperature of 52 °C. The tip of the laminate deflected approximately 35 mm vertically at this temperature as shown in Fig. 8(A). Then the current was turned off, leaving the plate to cool down and return to the initial configuration.

Table 1
Constant voltage testing data summary.

Test #	1	2	3
Volts [V]	16	30	16
Max R [Ω]	16.0	15.7	15.5
Min R [Ω]	14.3	14.2	13.8
On Time [s]	92	9	61
Max Temp [°C]	52	59	33
Max Tip Defl. [mm]	35	56	25

The voltage was increased to 30 V in test 2, inducing 1.9 A in the wire and heating it to a measured temperature of 59 °C. In this test, 56 mm maximum tip deflection was achieved as shown in Fig. 9(A), along with significant damage to the test sample. A loud audible crack was heard when maximum deflection was achieved and the tip deflection was drastically reduced after. After cooldown, a significant amount of negative tip deflection was observed.

A second 1.0 A test was attempted on the laminate after it had cooled from the prior test. In this last test (test 3), the laminate deflected up to only 25 mm before it finally buckled as shown in Fig. 10(A and B). The deflection was back to −9 mm after cooldown.

Images of the laminate before testing and after each test are shown in Fig. 11. Small cracks appeared around the wires after the laminate achieved the first 35 mm deflection test. These cracks are also shown in Fig. 12(A). These indications of damage appeared as small white blemishes, which the wire could not be seen through. They also could be felt by hand as they were slightly raised off the surface of the laminate. After undergoing 56 mm deflection, more of these cracks appeared. The epoxy around the wires also became opaquer, indicating the matrix was likely yielding around the wires. The delamination that occurred after buckling in test 3 is also clearly visible as a large white blemish in Fig. 12 (B).

6.2. Temperature sweep test results

A series of temperature sweep tests were conducted on laminates 2 and 3 using the temperature-based control method. Fig. 13 through Fig. 16 show the measured resistance, current, temperature, and tip deflection recorded in these sweep tests. Each test consisted of the laminate undergoing five heating and cooling cycles. In these tests the setpoint maximum temperatures were varied while resistance, current and tip deflection were measured. The DC power supply was set to provide a constant 24 V. To shorten the amount of time required to heat the wire, while still minimizing overshoot, the control scheme incorporated a two-step heating method. This method first allowed the maximum current (source voltage divided by wire resistance) to flow through the wire until the temperature reading approached a user-adjustable percentage of the set temperature. For example, in Fig. 13, the voltage across the wire was held constant until about three seconds into the test. In addition to reducing the amount of time to heat the wire, the constant voltage portion of the heating cycle also allowed for simpler measurement of the wire's resistance with each heating cycle. After the temperature reached 36 °C, or 80% of the setpoint of 45 °C, the controller entered a closed-loop control mode and began targeting its temperature setpoint. This occurred from 3 to 13 s in Fig. 13, in which the voltage across the SMA wire was varied by the controller and therefore varying the applied current. The duration of this closed-loop control holding period was also user-adjustable and was set to 10 s for all tests shown in this subsection. Measurement of the wire resistance during this part of the cycle was made difficult by the varying resistance across the current control MOSFET. Because resistance tended to reach a minimum within the first couple of seconds of each cycle, resistance measurements taken only over the constant voltage section in the first few seconds of the heating cycle was sufficient. After the closed-loop control holding period, current was shut off and the wire cooled to a user-adjustable percentage of room temperature before repeating the heating/cooling cycle. In these tests, this temperature was 32 °C.

The data presented in the shown figures was recorded during the fifth cycle of each test. This choice was based on the observation that the matrix and fibers in the laminate structure increased in temperature over the first few cycles of each test. With this increase in temperature, the maximum tip deflection at the end of the 10 s heating cycle also

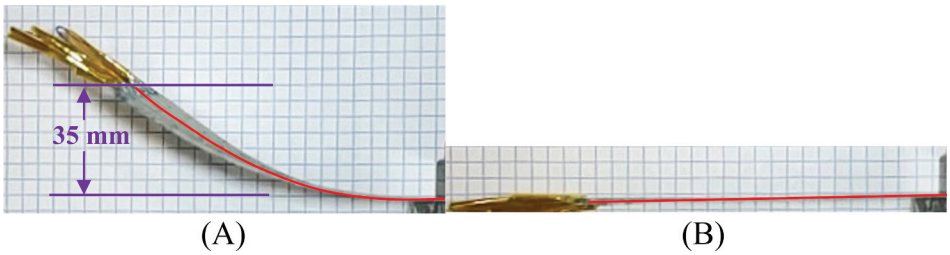

Fig. 8. Maximum deflection of 35 mm observed during 16 V test (A) and cooldown deflection (B).

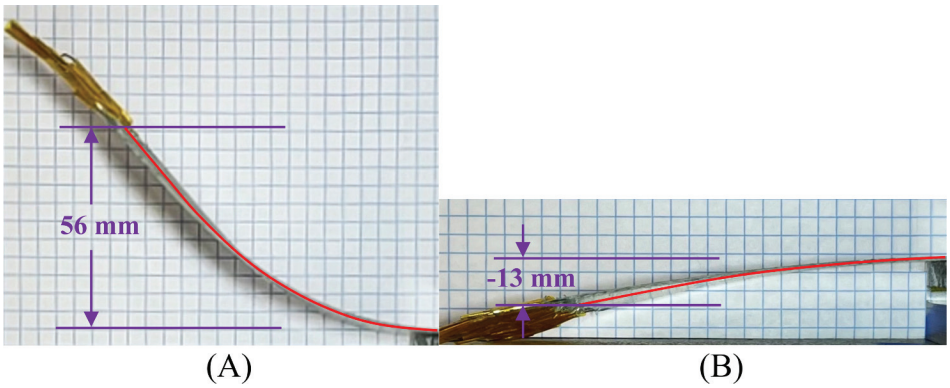

Fig. 9. Maximum vertical tip deflection of 56 mm (A) and post cooldown deflection of −13 mm (B).

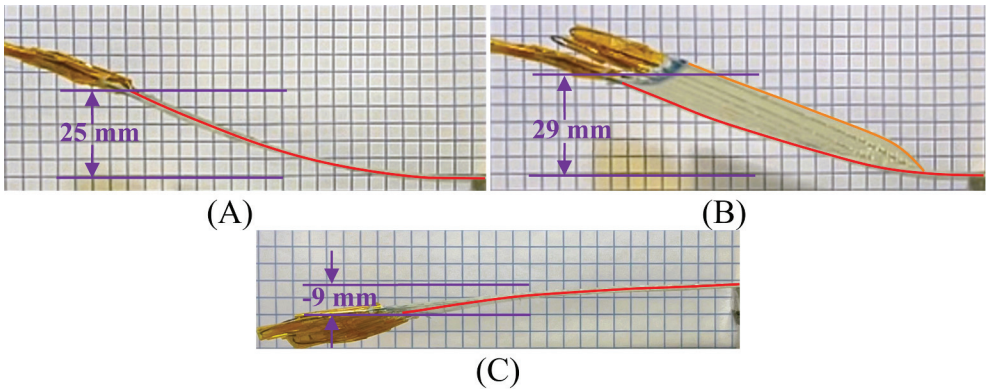

Fig. 10. Second 1.0 A test maximum vertical tip deflection of approximately 25 mm before buckling (A), post buckling (B), and −9 mm post cooldown (C).

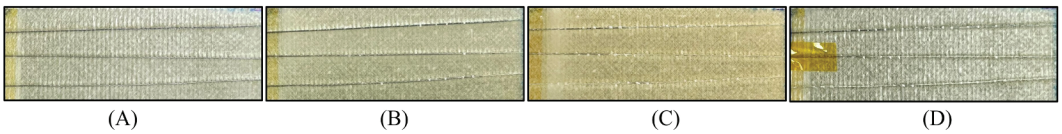

Fig. 11. Visual inspection pre-test (A), post 35 mm tip deflection (B), post 56 mm tip deflection (C), and post buckling at 25 mm tip deflection (D).

increased. The increase in temperature enables phase transformation, leading to an increase in the SMA wire's strain and stress. This increases the bending moment applied on the plate, resulting in higher tip deflections. A "cold start-up" effect was observed in which lower deflection values were achieved in the first two or three cycles because not enough heat was provided over the temperature control period to achieve the setpoint temperature. Therefore, the results shown in the plots better capture the steady state performance of the morphing composite. The cooling portion of the cycle ended at around 33 °C, above room temperature, which is why the deflection does not start at zero in the plots.

A mixture of overdamped and underdamped results was achieved during the temperature sweep tests. Because the controller was based on temperature readings, the terms "overdamped" or "underdamped" apply to the temperature recorded in each test mentioned in this section. The data shown in Fig. 13 illustrates an example of overdamped behavior because the wire temperature falls just short of the setpoint over the duration of the test. The tip deflection of the laminate increases quickly with time under maximum current until current control mode comes on at about three seconds, at which point the tip velocity (or the slope of the tip deflection curve) decreases. The tip deflection then increased steadily as the temperature increased until 13 s. At that point the current is switched off and the wire quickly cools, causing the tip deflection to

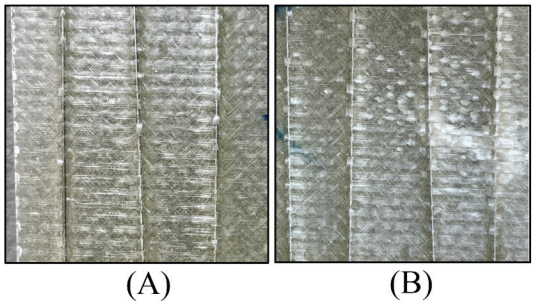

Fig. 12. Initial signs of debonding observed after the first 35 mm deflection cycle (A) and severe debonding after buckling (B).

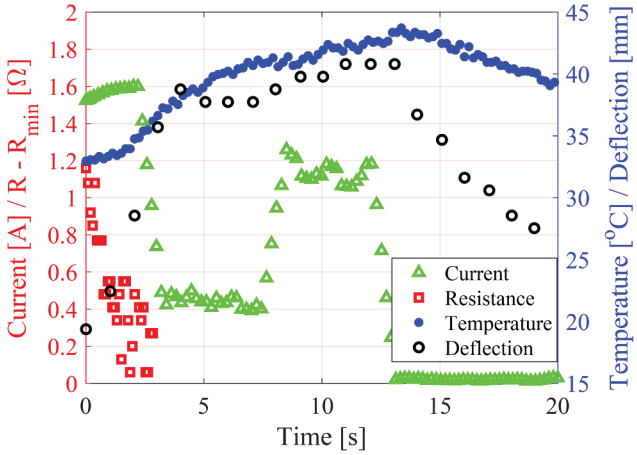

Fig. 13. Resistance, current, temperature and tip deflection measurements during heating cycle and beginning of cooling: 45 °C setpoint – Overdamped, Laminate 3.

reverse suddenly.

The data shown in Fig. 14 however presents a case of underdamped behavior in which the wire temperature exceeded the setpoint at around ten seconds. The current starts at around 1.0 A at the beginning of the current control mode and decreases to zero at the point that the temperature reaches 45 °C. The tip deflection also reaches a maximum of 55 mm at this point, but quickly falls to 43 mm over the two seconds the current is switched off. When the measured wire temperature drops under 45 °C, the current was switched back on to around 0.5 A and the tip deflection increased to 46 mm before the end of the 10-second temperature holding period.

The thermocouple tip required additional time to heat or cool, and thus the wire internal temperature achieved a maximum before the thermocouple tip. This is why maximum tip deflection was achieved before maximum measured temperature was achieved. In other words, the wire had a lower thermal inertia than the thermocouple which resulted in the embedded wires' actual internal temperature overshooting the intended setpoint. It also resulted in decreasing tip deflection even while the measured wire temperature remained relatively steady around the setpoint temperature.

The data shown in Fig. 15 present a case of overdamped temperature control. In this test, temperature control mode remained on for the entire ten seconds. This test is a good example of the effect of current on tip deflection. As the current gradually decreased while the measured wire temperature approached 48 °C, the tip velocity also decreased to zero, or in other words, held constant deflection at around ten seconds. At this point, the current was near the value required to maintain steady-state tip deflection, i_{SS}. The data in Fig. 15 show that about 1.0 A was required to maintain 57 mm tip deflection for laminate 3 while undergoing natural convection at room temperature.

Similarly, the data in Fig. 16 shows about 0.5 A is required to maintain a steady 18 mm tip deflection for laminate 2 under the same convective conditions. Because wire stress increases with increasing tip deflection, higher temperatures are required to induce additional strain recovery. The amount of current required to achieve steady state deflection also increases.

The effect of laminate stiffness can be observed from the data presented in Fig. 17 in which maximum tip deflection is plotted versus setpoint temperature for laminates 2 and 3. Laminate 3 achieved higher tip deflection values at every given temperature than laminate 2 due to its lower bending stiffness. This was a result of the transformation temperatures shifting upwards as stress increased in the SMA wire. Stress in the wire is developed at a lower rate in laminate 3 than in laminate 2 because all fibers are perpendicular to the wire, resulting in laminate 3 having the lowest bending stiffness in the actuation axis. This phenomenon presented itself in the varying deflection-temperature slopes for each laminate. The tip displacement sensitivity to temperature decreased in response to increasing stiffness.

Good correlation between temperature and tip deflection was observed with both laminates. The data points in each series with significantly lower tip deflection than the rest of the data at the same temperature are the "cold start-up" cycles from each test. In these cycles, the matrix was at room temperature and was not yet heated from successive cycling. After heating, the matrix was both less stiff and warmer,

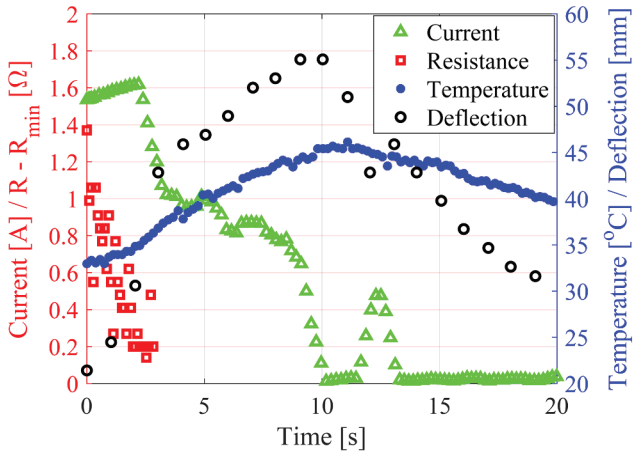

Fig. 14. Resistance, current, temperature and tip deflection measurements during heating cycle and beginning of cooling: 45 °C setpoint – Underdamped, Laminate 3.

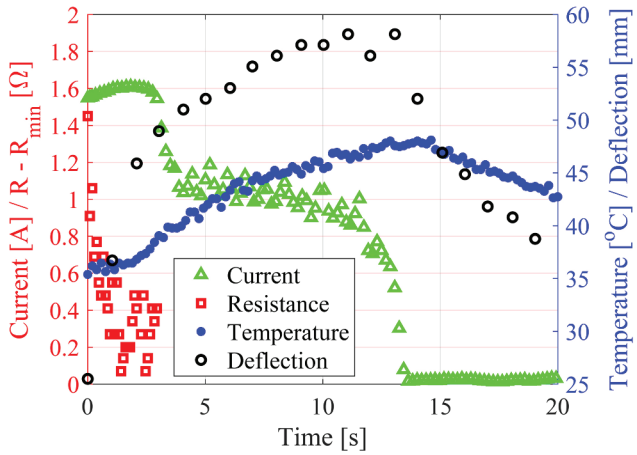

Fig. 15. Resistance, current, temperature and tip deflection measurements during heating cycle and beginning of cooling: 48 °C setpoint – Overdamped, Laminate 3.

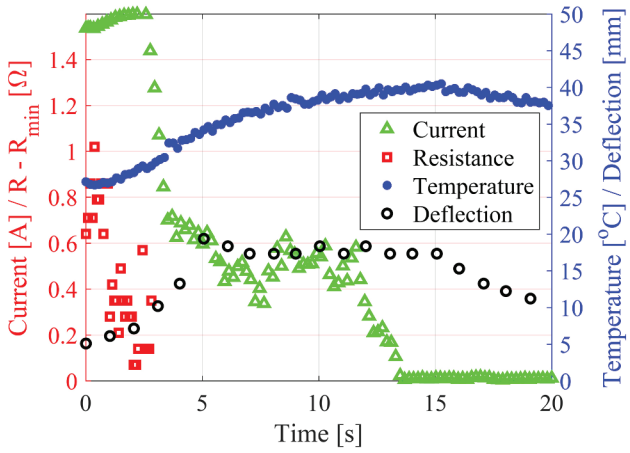

Fig. 16. Resistance, current, temperature and tip deflection measurements during heating cycle and beginning of cooling: 40 °C setpoint – Overdamped, Laminate 2.

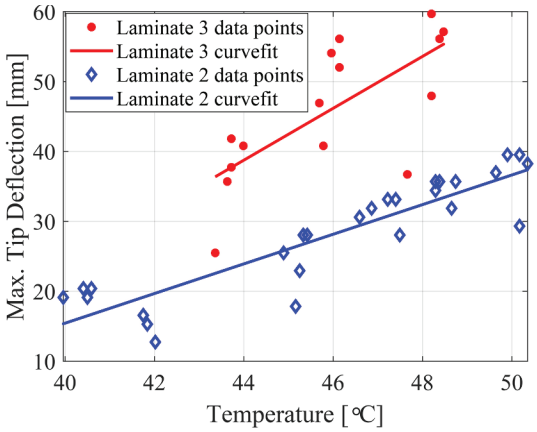

Fig. 17. Maximum tip deflection over various temperatures for laminates 2 and 3.

meaning it pulled less heat from the wire allowing it to achieve higher temperatures over the short test duration.

6.3. Cycle testing results

After temperature sweep testing, both laminates 2 and 3 were subjected to repeated-cycle testing. In these tests, both laminates completed 1000 heating and cooling cycles between setpoint maximum and minimum temperatures. Deflection and temperature data recorded during observed cycles from these tests are shown in Fig. 18 and Fig. 19. All recorded cycles show both "start deflection" and "end deflection" values which represent the tip deflection recorded at the beginning and end of the temperature control period. The temperature controller was set in both tests so that the position and temperature control was overdamped. This way, maximum tip deflection occurred when maximum temperature was achieved.

The temperature control system was found to be sensitive to ambient temperature, convection boundary conditions, and residual heat in the system, therefore some variations in maximum temperature achieved during each cycle occurred. This resulted in some tip deflection variation from cycle to cycle, as in the case of laminate 2 shown in Fig. 19. A large increase in deflection, seen around 200 cycles, was caused by removing a fan that had been blowing air over the laminate to decrease the cooling time in between cycles. This was done to investigate the effect of the convection boundary conditions on the tip deflection. After

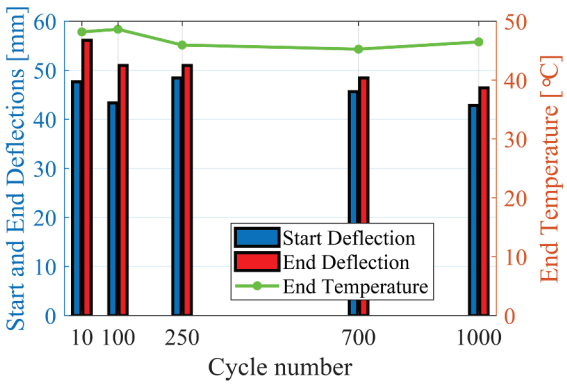

Fig. 18. Laminate 3 tip deflection at start and end of temperature control sequence and maximum measured temperature during observed cycles.

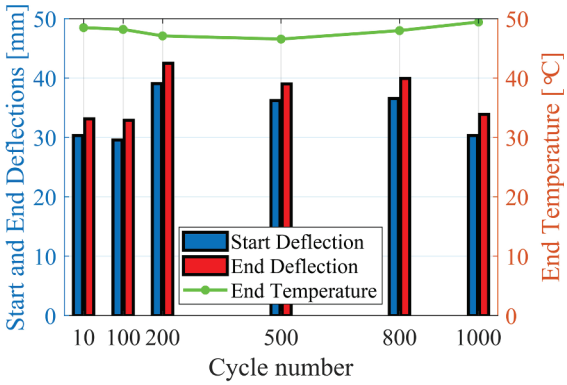

Fig. 19. Laminate 2 tip deflection at start and end of temperature control sequence and maximum measured temperature during observed cycles.

noticing that deflection had increased significantly over a few cycles, the fan was replaced. This disturbance in the test setup demonstrated the sensitivity of the morphing composite to convection boundary conditions, an observation that was recently reported by Choyal *et al.* [19].

Though both laminates remained intact and operational for the duration of the respective 1000 cycle tests, each laminate incurred visibly detectable damage. In both tests, no fiber breakage was observed visually nor audibly. In the case of laminate 3, yielding of the matrix resulted in significant permanent tip deformation. This yielding continued throughout cycle testing until a permanent tip deflection of 15 mm was incurred at room temperature. Damage to laminate 3 was also observed in the overhead visual inspection images provided in Fig. 20. Cracking, similar to that seen with laminate 1, was observed on the surface on the compression side of the laminate.

Laminate 2 also incurred noticeable damage throughout cycle testing, as shown in Fig. 21. Permanent tip deformation occurred during the temperature sweep testing, which implies that stresses encountered at maximum deflection in these tests were beyond the safe operating limits of the flexible epoxy. This permanent positive tip deformation continued until it was noted that after the completion of 800 cycles, it had reversed and become negative, similar to what had occurred with laminate 1. In both laminates 1 and 2, fibers were placed at an angle to the wire such that they added stiffness in the bending direction. Given the wire stresses are high, it is likely that some degree of permanent deformation was occurring in the SMA wire.

7. Conclusions

Embedding SMA wires in flexible composite laminates can enable the design of a variety of interesting applications involving active plates and

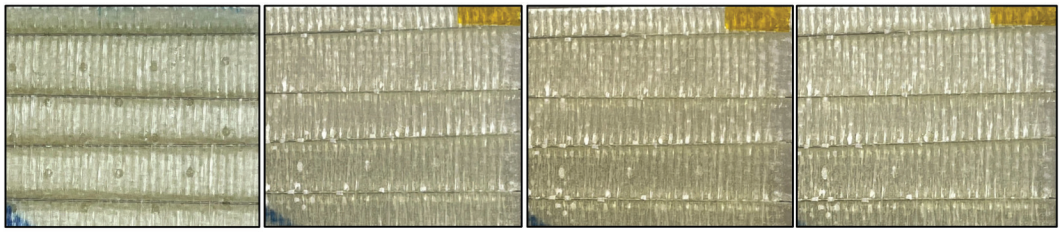

Fig. 20. Visual inspection of laminate 3 before testing (A), after 100 (B), 700 (C), and 1000 cycles (D).

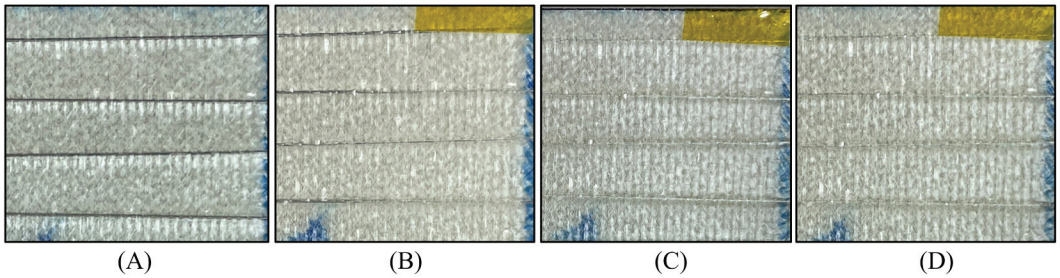

Fig. 21. Visual inspection of laminate 2 before testing (A), post temperature sweep testing (B), after 800 (C), and 1000 cycles (D).

shells. This paper focused on different experimental aspects of flexible laminated composite plates with embedded SMA wires. Dynalloy's 0.38 mm diameter FLEXINOL wires were sanded and embedded in a Hex-Force™ 7715 unidirectional fiberglass three-ply laminates with Rhino 1382 low modulus flexible epoxy resin. Three proof-of-concept samples were manufactured with varying fiber-orientation angles relative to the embedded parallel SMA wires. Various tests were performed on the square plate samples in a cantilever configuration. Laminate 1 with [90°/W/-45°/45°] stacking sequence was subjected to constant voltage tests to investigate the nature of damage that could occur. As the applied electric current increased, the SMA wires' temperature increased, and started yielding the matrix around the wires and debonding. At high enough temperature, the damage between neighboring wires propagated and caused sudden delamination, accompanied by audible sound, and permanent damage. Upon cooldown the laminate acquired negative deflection and further actuation led to buckling and lower tip deflection.

Lamiantes 2 and 3, with [90°/W/-60°/60°] and [90°/W/90°/90°] stacking sequence, respectively, were subjected to cyclic loadings. The developed temperature-based control method proved to be accurate and robust despite the large size of the thermocouple head used to measure the SMA wire temperature. As expected, the effect of the fiber-orientation angle of the composite plies showed to be significant on the stiffness of the structure and accordingly the tip deflection. Although both laminates were able to undergo 1000 actuation cycles with small variation in tip deflection, damage around the wires was seen as the laminates underwent hundreds of cycles. Convection boundary conditions affected the tip deflection significantly, thus future iterations of the wire temperature control circuit should be adaptive to changes in the surroundings of the smart composite plates.

Data availability

The raw and processed data required to reproduce these findings are available from the corresponding author on reasonable request.

CRediT authorship contribution statement

Andrew Theodore: Conceptualization, Methodology, Software, Validation, Formal analysis, Investigation, Resources, Data curation, Writing – original draft, Writing – review & editing, Visualization, Project administration, Funding acquisition. **Peter L. Bishay:** Conceptualization, Methodology, Validation, Formal analysis, Investigation, Resources, Data curation, Writing – original draft, Writing – review & editing, Visualization, Supervision, Project administration, Funding acquisition.

Declaration of Competing Interest

The authors declare that they have no known competing financial interests or personal relationships that could have appeared to influence the work reported in this paper.

Acknowledgments

The authors acknowledge the support of California State University, Northridge (CSUN), and the "Thesis/Project/Dissertation Support Program" grant received in 2020 from CSUN's office of graduate studies.

References

[1] Bil C, Massey K, Abdullah EJ. Wing morphing control with shape memory alloy actuators. J Intell Mater Syst Struct 2013;24(7):879–98. https://doi.org/10.1177/1045389X12471866.
[2] Basaeri H, Yousefi-Koma A, Zakerzadeh MR, Mohtasebi SS. Experimental study of a bio-inspired robotic morphing wing mechanism actuated by shape memory alloy wires. Mechatronics 2014;24(8):1231–41. https://doi.org/10.1016/j.mechatronics.2014.10.010.
[3] Bishay PL, Finden R, Recinos S, Alas C, Lopez E, Aslanpour D, et al. Development of an SMA-based camber morphing UAV tail core design. Smart Mater Struct 2019;28(7):075024. https://doi.org/10.1088/1361-665X/ab1143.
[4] Wang W, Ahn S-H. Shape memory alloy-based soft gripper with variable stiffness for compliant and effective grasping. Soft Rob 2017;4(4):379–89. https://doi.org/10.1089/soro.2016.0081.
[5] Lee JH, Chung YS, Rodrigue H. Long shape memory alloy tendon-based soft robotic actuators and implementation as a soft gripper. Sci Rep 2019;9:1–12. https://doi.org/10.1038/s41598-019-47794-1.
[6] Bishay PL, Fontana J, Raquipiso B, Rodriguez J, Borreta MJ, Enos B, et al. Development of a biomimetic transradial prosthetic arm with shape memory alloy muscle wires. Engineering Research Express 2020;2(3):035041. https://doi.org/10.1088/2631-8695/abb710.
[7] Bishay PL, Aguilar C, Amirbekyan A, Vartanian K, Arjon-Ramirez M, Pucio DB. Design of a lightweight shape memory alloy stroke-amplification and locking system in a transradial prosthetic arm. In: ASME conference on smart materials, adaptive atructures and intelligent systems (SMASIS), September 14-15; 2021. https://doi.org/10.1115/SMASIS2021-68248.

[8] Cohades A, Michaud V. Shape memory alloys in fibre-reinforced polymer composites. Advanced Industrial and Engineering Polymer Research 2018;1(1):66–81. https://doi.org/10.1016/j.aiepr.2018.07.001.
[9] Ellis R. Ballistic impact resistance of graphite epoxy composites with shape memory alloy and extended chain polyethylene spectra hybrid components (19735). Master Thesis, Virginia Polytechnic Institute and State University. VTechWorks, 1996.
[10] Guida M, Marulo F, Russo S. NiTi SMA wires coupled with Kevlar fabric: A real application of an innovative aircraft LE slat system in SMAHC material. Appl Compos Mater 2018;25(2):269–98. https://doi.org/10.1007/s10443-017-9618-4.
[11] Pappadà S, Gren P, Tatar K, Gustafson T, Rametta R, Rossini E, et al. Mechanical and vibration characteristics of laminated composite plates embedding shape memory alloy superelastic wires. J Mater Eng Perform 2009;18(5–6):531–7. https://doi.org/10.1007/s11665-009-9403-0.
[12] Viet NV, Zaki W. Analytical investigation of the behavior of concrete beams reinforced with multiple circular superelastic shape memory alloy bars. Compos Struct 2019;210:958–70. https://doi.org/10.1016/j.compstruct.2018.11.080.
[13] Viet NV, Zaki W, Umer R. Analytical model of functionally graded material/shape memory alloy composite cantilever beam under bending. Compos Struct 2018;203:764–76. https://doi.org/10.1016/j.compstruct.2018.07.041.
[14] Viet NV, Zaki W. Bending model for a laminated composite cantilever beam with multiple embedded shape memory alloy layers presenting tensile-compressive asymmetry. Compos Struct 2019;229:111410. https://doi.org/10.1016/j.compstruct.2019.111410.
[15] Kirkby EL, Rule JD, Michaud VJ, Sottos NR, White SR, Månson J-A. Embedded shape-memory alloy wires for improved performance of self-healing polymers. Adv Funct Mater 2008;18(15):2253–60. https://doi.org/10.1002/adfm.200701208.
[16] Kirkby EL, Michaud VJ, Månson J-A-E, Sottos NR, White SR. Performance of self-healing epoxy with microencapsulated healing agent and shape memory alloy wires. Polymer 2009;50(23):5533–8. https://doi.org/10.1016/j.polymer.2009.05.014.
[17] Han M-W, Rodrigue H, Kim H-I, Song S-H, Ahn S-H. Shape memory alloy/glass fiber woven composite for soft morphing winglets of unmanned aerial vehicles. Compos Struct 2016;140:202–12. https://doi.org/10.1016/j.compstruct.2015.12.051.
[18] Han M, Kim M, Ahn S. Shape memory textile composites with multi-mode actuations for soft morphing skins. Compos B 2020;198:1–10. https://doi.org/10.1016/j.compositesb.2020.108170.
[19] Choyal V, Khan S, Mani PSS, Palani IA, Singh P. Active and passive multicycle actuation characteristics of shape memory alloy-based adaptive composite structures. Smart Mater Struct 2021;30(9):095022. https://doi.org/10.1088/1361-665X/ac177d.
[20] Kim H-I, Han M-W, Song S-H, Ahn S-H. Soft morphing hand driven by SMA tendon wire. Compos B 2016;105:138–48. https://doi.org/10.1016/j.compositesb.2016.09.004.
[21] Bishay PL, Sofi AR. Sensitivity analysis of a smart soft composite robotic finger design using geometrically nonlinear laminated composite finite beam elements. Mater Today Commun 2018;16:111–8. https://doi.org/10.1016/j.mtcomm.2018.05.004.
[22] Daghia F. Active fibre-reinforced composites with embedded shape memory alloys. Universita di Bologna; 2008. Doctoral Thesis.
[23] Leal P, Stroud H, Sheahany E, Cabraly M, Hartl D. Skin-based camber morphing utilizing shape memory alloy composite actuators in a wind tunnel environment. In: 26th AIAA/AHS adaptive structures conference, Kissimmee, Florida; January 2018. https://doi.org/10.2514/6.2018-0799.
[24] Jin Hu, Dong E, Xu M, Liu C, Alici G, Jie Y. Soft and smart modular structures actuated by shape memory alloy (SMA) wires as tentacles of soft robots. Smart Mater Struct 2016;25(8):085026. https://doi.org/10.1088/0964-1726/25/8/085026.
[25] Wang W, Rodrigue H, Ahn S-H. Smart soft composite actuator with shape retention capability using embedded fusible alloy structures. Compos B Eng 2015;78:507–14. https://doi.org/10.1016/j.compositesb.2015.04.007.
[26] Lau K-T, Chan A-L, Shi S-Q, Zhou L-M. Debond induced by strain recovery of an embedded NiTi wire at a NiTi/epoxy interface: micro-scale observation. Mater Des 2002;23(3):265–70. https://doi.org/10.1016/S0261-3069(01)00087-5.
[27] Yuan G, Bai Y, Jia Z, Hui D, Lau K-T. Enhancement of interfacial bonding strength of SMA smart composites by using mechanical indented method. Compos B 2016;106:99–106. https://doi.org/10.1016/j.compositesb.2016.08.033.
[28] Yuan G, Bai Y, Jia Z, Lau K-T, Hung P-Y. Structural deformation performance of glass fiber reinforced polymer composite beam actuated by embedded indented SMA wires. Compos B 2019;159:284–91. https://doi.org/10.1016/j.compositesb.2018.09.101.
[29] Lester BT, Baxevanis T, Chemisky Y, Lagoudas DC. Review and perspectives: shape memory alloy composite systems. Acta Mech 2015;226(12):3907–60. https://doi.org/10.1007/s00707-015-1433-0.
[30] Merlin M, Scoponi M, Soffritti C, Fortini A, Rizzoni R, Garagnani G. On the improved adhesion of NiTi wires embedded in polyester and vinyl-ester resins. Frattura ed Integrità Strutturale 2015;9:127–37. https://doi.org/10.3221/IGF-ESIS.31.10.
[31] Rhino Linings Corporation. Rhino™ 1382 Low Modulus Flexible Epoxy Resin Data Sheet, 2009.
[32] Zheng YJ, Cui LS, Schrooten J. Basic design guidelines for SMA/epoxy smart composites. Mater Sci Eng, A 2005;390(1–2):139–43. https://doi.org/10.1016/j.msea.2004.07.063.
[33] Daniel I, Ishai O. Engineering Mechanics of Composite Materials (2nd Edition). Taylor & Francis; 2006.
[34] Lin K. Composite Materials: Materials, Manufacturing, Analysis, Design and Repair. CreateSpace; 2015.
[35] Broughton W. Adhesives in Marine Engineering. Woodhead Publishing; 2012.
[36] Smith NA, Antoun GG, Ellis AB, Crone WC. Improved adhesion between nickel–titanium shape memory alloy and a polymer matrix via silane coupling agents. Compos A Appl Sci Manuf 2004;35(11):1307–12. https://doi.org/10.1016/j.compositesa.2004.03.025.
[37] Jonnalagadda K, Kline GE, Sottos NR. Local displacements and load transfer in shape memory alloy composites. Exp Mech 1997;37(1):78–86. https://doi.org/10.1007/BF02328753.
[38] Rey T, Razan F, Robin E, Faure S, Le Cam J-B, Chagnon G, et al. Mechanical characterization and comparison of different NiTi/silicone rubber interfaces. Int J Adhes Adhes 2014;48:67–74. https://doi.org/10.1016/j.ijadhadh.2013.09.028.
[39] Cengel Y, Ghajar A. Heat and Mass Transfer: Fundamentals and Applications. (5th Edition). McGraw-Hill Higher Education; 2014.